IEEE Access
Multidisciplinary | Rapid Review | Open Access Journal

Received October 19, 2019, accepted October 30, 2019, date of publication November 4, 2019, date of current version November 14, 2019.

Digital Object Identifier 10.1109/ACCESS.2019.2951224

Three-Dimensional Transient Electromagnetic Numerical Simulation Using FDFD Based on Octree Grids

HUI LUAN[1,2], YINAN GENG[1], YIBING YU[1], AND SHANSHAN GUAN[1,2]
[1]Department of Instrumentation and Electrical Engineering, Jilin University, Changchun 130026, China
[2]Key Laboratory of Geophysical Exploration Equipment, Ministry of Education, Jilin University, Changchun 130026, China

Corresponding author: Shanshan Guan (guanshanshan@jlu.edu.cn)

This work was supported in part by the Natural Fund Project for Jilin Province under Grant 20160101265JC, in part by the National Natural Science Foundation of China under Grant 41604084, and in part by the Research Planning Projects of Science and Humanities in Universities of the Education Department of Jilin Province under Grant JJKH20190127KJ.

ABSTRACT The transient electromagnetic method (TEM) has been widely used as a geophysical exploration method in recent years. When Maxwell's equations are discretized in the time domain by the direct solution method, the initial field is used as a substitute for the source, so the electromagnetic response of a shallow three-dimensional anomalous body cannot be calculated. Maxwell's equations in the frequency domain are simple in form, and the current source can be directly added without calculating the initial field. However, large linear equations must be calculated. The coefficient matrix is large, and the calculation speed is slow, which limits their application. Based on Yee grids, this paper combines octree grids with the finite-difference frequency-domain (FDFD) method. Ensuring a sufficiently large computational area, octree grids are used to refine the area of anomalous bodies, while coarse grids are still used to reduce the total number of grids and improve the efficiency. In the numerical simulation, the vacancy positions are set to zero to solve the data storage problem of the coarse grids and fine grids. The binary paraboloid interpolation method is used to solve the electromagnetic field component transfer problem at the intersection of the coarse grid and fine grid. Finally, the electromagnetic response curve in the time domain is obtained by a frequency-time transformation. By comparing the calculation results of typical models, the correctness of the FDFD method based on octree grids is verified. By comparing the computational time of complex anomalous bodies for Yee grids and octree grids, it can be concluded that the efficiency of the FDFD method based on octree grids is improved to a certain extent.

INDEX TERMS Finite-difference frequency-domain (FDFD), frequency-time transformation, numerical simulation, octree grids, transient electromagnetic method (TEM).

I. INTRODUCTION

The transient electromagnetic method (TEM) is a detection method based on the principle of electromagnetic induction, which can be used to detect the resistivity of underground nonmagnetic materials. The TEM is widely used in many fields, such as metal resources, groundwater, underground unexploded ordnance and urban underground space [1]. The numerical simulation methods of the TEM mainly include the finite-difference method [2], finite element method [3], mesh-free method [4], finite volume method [5] and integral equation method [6]. Compared with other numerical simulation methods, the finite-difference method transforms differential equations into difference equations [7]. The principle is simple and intuitive, and the reliability is high. Other methods can also be compared with the finite-difference method for verification. Finite-difference numerical simulation methods are mainly divided into two kinds: the finite-difference time-domain (FDTD) method and the finite-difference frequency-domain (FDFD) method [8]. The FDTD method iterates successively according to the time step, which is easy to understand. With numerous studies, the FDTD method has developed rapidly. Some high-order strategies have been used to improve stability [9]. However, in the calculation process,

The associate editor coordinating the review of this manuscript and approving it for publication was Mehmet Alper Uslu.

the FDTD algorithms mostly calculate the initial field and the iterated field separately. Therefore, it is difficult to change the source type directly. As the initial field is calculated in a uniform half-space model, an anomalous body cannot be placed in a certain range of earth, which limits its application. The FDFD method has been developed for a long time, and its technology is mature. Thus, the FDFD method has been used to perform many numerical simulations for ground and space exploration, and it is still being used in various electromagnetic field analyses [10]–[12]. In geophysics, based on Yee grids, Hedlin [13] used the FDFD method for magnetotelluric numerical simulation. Then, he analyzed the influence of grid spacing on the calculation error and deduced the corresponding error expression. Yoon [14] combined FDFD with the integral equation method for numerical simulation of marine controllable sources. First, the electric field component is calculated by the FDFD method, and then the magnetic field at the receiver is calculated accurately by the integral equation method to reduce the computational complexity. Li [15] used the FDFD method for numerical simulation of marine controllable sources. The interpolation method is used in the receiving point area of the rugged seabed to obtain the precise position and improve the calculation accuracy. However, there are few studies on grid refinement methods to improve the computational efficiency. Without considering the stability condition, a solution to the FDFD method always exists if the coefficient matrix rank is full. In addition, each frequency point can be solved independently, which is convenient for parallel acceleration. However, this method has one obvious disadvantage: the response of each frequency point needs to solve large linear equations, which takes a long time, especially for three-dimensional forward modeling [16]. By analyzing the calculation process of linear equations, the number of grids directly affects the size of the coefficient matrix, which is the key factor of the calculation time. When analyzing complex anomalous bodies, we need to use smaller-scale grids. To maintain a sufficiently large computing area, more grids should be used, which increases the computing time.

To solve the above problems, based on Yee grids [17], some scholars use fine grids to refine anomalous bodies. While the coarse grid size is kept constant, the minimum grid size is reduced. In the research of FDTD numerical simulation, the subgridding technique can be used to refine the region where the anomalous body is located. Specifically, the electromagnetic fields on the coarse grid iterate from time n to time n+1 in the normal way. Then the electromagnetic fields on the boundary of the coarse girds and fine grids are obtained by interpolating that on the coarse grid at time n. Finally, the electromagnetic fields on the fine grid iterate to time n+1 separately and update that on the coarse grid. The process is repeated continuously [18]–[19]. For the FDFD method, because the responses of each frequency point are obtained by solving the linear equations directly, it is difficult to calculate the refined region separately by the subgridding technique. Therefore, we use octree grids to refine the region where the anomalous body is located. Octree grids are very flexible and are mostly used in the numerical simulations of the finite volume method [20] and the FDTD method [21]. Due to its finer grid, octree grids are widely used in many fields, such as hydrodynamics [22], electromagnetics [23]–[24] and seismic waves [25]. Haber and Heldmann [23] deduced the integral form of Maxwell's equations with the finite volume method based on octree grids and used the flux conservation method to connect the components in different grids. Theillard [26] used Dirichlet boundary conditions and analyzed the discrete form of Poisson's equation in the time domain based on octree grids. Min *et al.* [27] used a second-order accurate finite-difference discretization for Poisson's equation. Yin [28] deduced the binary paraboloid interpolation method and studied the microstructure simulation of alloy solidification based on octree grids. Raeli *et al.* [29] used a difference scheme for Poisson's equation based on octree grids and optimized the truncation error. Chernyshenko *et al.* [30] used a finite volume method based on octree grids to analyze the diffusion process in porous media. Valente *et al.* [20] developed a useful finite volume method using octree grids to simulate hyperthermia treatment. Octree grids are widely used in many fields; however, there are few relevant studies on geophysical problems solved by the three-dimensional FDFD method based on octree grids.

In this paper, we study how to apply octree grids to the FDFD numerical simulation method. To solve the problem of the electromagnetic field component transfer between grids of different scales, the binary paraboloid interpolation method is used to obtain the required magnetic field components. According to the data structure used by Horesh with the finite volume method, based on fine grids, the vacancy positions of each component of a coarse grid are set to zero. To reduce the computational complexity, the zero vector does not participate in the actual operations. The efficiency is obtained by analyzing the calculation time of an L-shaped anomalous body and a trapezoid anomalous body. For complex anomalous bodies, such as those with inclined or sharp angles, it is possible to subdivide the irregular parts only. Although this is not completely equivalent to an inclined plane, the effect of fine grids is better than that of coarse grids. The electromagnetic response curve in the time domain is obtained by a frequency-time transformation. Comparing the computational time of the FDFD method based on Yee grids with that based on octree grids, the rationality of the application of the octree grids to the FDFD method is analyzed.

II. THEORY AND METHOD

In this paper, a three-dimensional finite-difference forward modeling method based on octree grids in the frequency domain is studied. Using the Yee grid scheme, the electromagnetic field components are discretized in the frequency domain. Variable step-size grids are used in the peripheral region to maintain a sufficiently large computational area. Uniform grids are used in the central region, and octree grids are used in the region where the anomalous body is located.

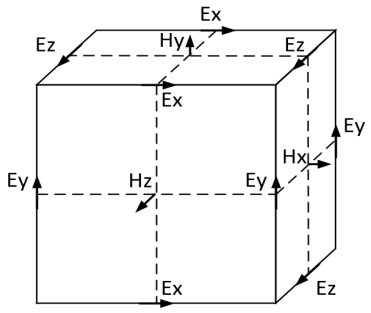

FIGURE 1. Yee grid.

In other words, different scale grids are used throughout the computational area. Coarse grids can be used to simulate the conductivity of the earth background and large regular anomalous bodies, while fine grids can be used to simulate complex anomalous bodies. Because the inner part of the octree grids conforms to the Yee grid structure, the difference condition of the Yee grid is still satisfied. Above all, as the FDFD method based on octree grids can ensure that the size of grid meets the requirement for subdivision of the anomalous body, the method can also reduce the total number of grids and the scale of the coefficient matrix. Then, the computational time could be reduced.

A. THREE-DIMENSIONAL FDFD NUMERICAL SIMULATION THEORY

Normally, the displacement current can be ignored when the frequency of the source is less than 1 MHz [16]. Thus, Maxwell's equations in the frequency domain can be expressed as

$$\nabla \times \mathbf{E} = -i\omega\mu_0\mathbf{H}, \tag{1}$$
$$\nabla \times \mathbf{H} = \sigma\mathbf{E} + \mathbf{J}, \tag{2}$$
$$\nabla \cdot \mathbf{E} = 0, \tag{3}$$
$$\nabla \cdot \mathbf{H} = 0. \tag{4}$$

where $\mathbf{E}$ is the electric intensity (V/m), $\mathbf{H}$ is the magnetic intensity (A/m), σ is the conductivity (S/m), μ_0 is the permeability of the vacuum (H/m), ω is the angular frequency and $\mathbf{J}$ is the conductive current density.

When equations (1) and (2) are solved simultaneously, considering the singularity of the source in the equation, the solution is difficult. Therefore, we can substitute equation (1) into equation (2) and obtain an equation that only depends on the electric field $\mathbf{E}$,

$$\nabla \times \nabla \times \mathbf{E} + i\omega\mu_0\sigma\mathbf{E} = -i\omega\mu_0\mathbf{J}. \tag{5}$$

Equation (5) contains only one unknown quantity, the electric field $\mathbf{E}$, which reduces the solution difficulty.

Equations (1) and (2) are discretized on the grid according to the Yee grid shown in Fig. 1. Four electric fields surround each magnetic field, and four magnetic fields surround each electric field. Then we can obtain equations

$$\mathbf{C_{EzDy}E_z} - \mathbf{C_{EyDz}E_y} = -i\omega\mu_0\mathbf{H_x}, \tag{6}$$
$$\mathbf{C_{ExDz}E_x} - \mathbf{C_{EzDx}E_z} = -i\omega\mu_0\mathbf{H_y}, \tag{7}$$
$$\mathbf{C_{EyDx}E_y} - \mathbf{C_{ExDy}E_x} = -i\omega\mu_0\mathbf{H_z}, \tag{8}$$
$$\mathbf{C_{HzDy}H_z} - \mathbf{C_{HyDz}H_y} = \sigma\mathbf{E_x} + \mathbf{J_x}, \tag{9}$$
$$\mathbf{C_{HxDz}H_x} - \mathbf{C_{HzDx}H_z} = \sigma\mathbf{E_y} + \mathbf{J_y}, \tag{10}$$
$$\mathbf{C_{HyDx}H_y} - \mathbf{C_{HxDy}H_x} = \sigma\mathbf{E_z} + \mathbf{J_z}. \tag{11}$$

$\mathbf{C_{ExDy}}$, $\mathbf{C_{ExDz}}$, $\mathbf{C_{EyDx}}$, $\mathbf{C_{EyDz}}$, $\mathbf{C_{EzDx}}$ and $\mathbf{C_{EzDy}}$ are six difference matrices of the electric fields, which represent the differential approach of the electric field components $\mathbf{E_x}$, $\mathbf{E_y}$ and $\mathbf{E_z}$ in different directions. $\mathbf{C_{HxDy}}$, $\mathbf{C_{HxDz}}$, $\mathbf{C_{HyDx}}$, $\mathbf{C_{HyDz}}$, $\mathbf{C_{HzDx}}$ and $\mathbf{C_{HzDy}}$ are six difference matrices about magnetic fields, which represent the differential approach of the magnetic field components $\mathbf{H_x}$, $\mathbf{H_y}$ and $\mathbf{H_z}$ in different directions. The conductivity on the edge of a grid can be averaged by four adjacent cubes. For a loop source, we only need to assign values to the source vectors of $\mathbf{J_x}$ and $\mathbf{J_y}$, as $\mathbf{J_z}$ is always a zero vector. According to equation (5), we substitute equations (6) to (8) into equations (9) to (11); then, we can obtain equations (12) to (14), as shown at the bottom of the next page. According to $\mathbf{Ax} = \mathbf{b}$, the components in equations (12) to (14) can be expressed as equations (15) to (17), as shown at the bottom of the next page.

Finally, we can calculate $\mathbf{x}$ to obtain the electric field $\mathbf{E}$. According to equations (6) to (8), we can obtain magnetic field $\mathbf{H}$. Calculating the electromagnetic response for 70 frequency points in the range of 0.1 Hz-1 MHz, we can use frequency-time conversion to obtain an electromagnetic response curve in the time domain by digital filtering [6].

B. OCTREE DATA STRUCTURE AND INTERPOLATION

The structure of octree grids is different from that of Yee grids, as shown in Fig. 2. Considering that the number of components in each direction is different for coarse and fine grids, the magnetic field $\mathbf{H}$, electric field $\mathbf{E}$ and grid size $\mathbf{S}$ are difficult to sort and store in normal order. To solve this problem, referencing Horesh's [24] storage format for each component of the octree grids used in the finite volume method, we store the grid size as shown in Fig. 2, where $\mathbf{S}(:,:,i)$ represents layer i in the octree grids. To be more specific, a coarse grid can be regarded as the combination of eight fine grids, so the storage space of a coarse grid is the same as that of eight fine grids. The grid size, electric field and magnetic field of the coarse grid are stored in the upper left corner of the data matrix, and the remaining vacancy positions are filled by 0. Equations (18) to (20) represent the storage of the electric field, and the matrix of the magnetic field is similar to that of the electric field. In this way, the data storage problem of the octree grid in the frequency domain is solved, and the location of each component is easy to sort and locate.

$$\mathbf{E}(:,:,1) = \begin{bmatrix} E_x & 0 & E_x & E_x \\ 0 & 0 & E_x & E_x \\ E_x & 0 & E_x & E_x \end{bmatrix}, \tag{18}$$
$$\mathbf{E}(:,:,2) = \begin{bmatrix} 0 & 0 & E_x & E_x \\ 0 & 0 & E_x & E_x \\ 0 & 0 & E_x & E_x \end{bmatrix}, \tag{19}$$

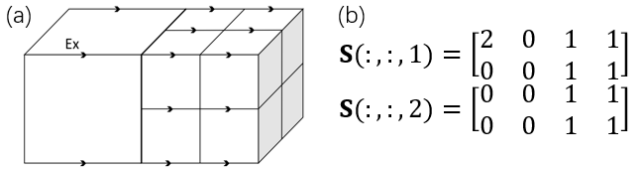

FIGURE 2. Octree structure and its representation. (a) Octree grid. (b) Data structure.

$$\mathbf{E}(:,:,3) = \begin{bmatrix} E_x & 0 & E_x & E_x \\ 0 & 0 & E_x & E_x \\ E_x & 0 & E_x & E_x \end{bmatrix}. \tag{20}$$

Because the vacancy positions of the components in the octree grid are filled by 0, the data matrix is large and sparse, which increases the volume of data and makes the matrix difficult to calculate. According to the Maxwell difference equations in the frequency domain, when the coefficient matrix **A** is full rank, a solution of the equation set always exists. After calculating the electric field difference matrix and the magnetic field difference matrix, we can obtain the coefficient matrix **A**. The number and location of the electric field component **E** are determined by the electric field storage matrix. Then, we need to delete all the zero rows and all the zero columns of the coefficient matrix **A**, which can reduce the amount of calculation and improve the efficiency of the solution. After the calculation, we add zero elements to the solution to obtain the three-dimensional array form of the electric field component for analysis.

Employing octree grids needs to solve the problem of the transmission of different components between the coarse and fine grids in the FDFD method. Unlike Yee grids, which only set boundary conditions at the outermost layer of the computational region, we should set a new boundary condition between the coarse and fine grids. More specifically, it is necessary to interpolate the electric field and magnetic field at the boundary of the coarse grids and fine grids, as shown in Fig. 3. When calculating the magnetic field by the electric

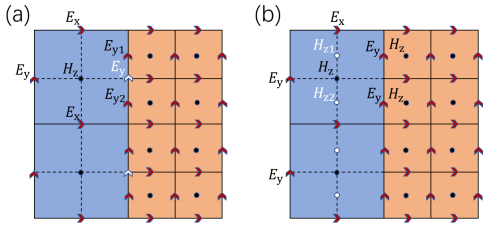

FIGURE 3. Interpolation method of electromagnetic fields. (a) The interpolation of electric fields. (b) The interpolation of magnetic fields.

field, all the magnetic field H_z on the right fine grids of Fig. 3a can be calculated by the difference between E_x and E_y. However, the magnetic field H_z of the left coarse grids lacks the surrounded electric field E_y (white letter) at the junction of the coarse and fine grids, so it cannot satisfy the difference scheme. Then, we averaged E_{y1} and E_{y2} on the right small grids to obtain E_y on the left coarse grid, that is

$$E_y = (E_{y1} + E_{y2})/2. \tag{21}$$

Similarly, when calculating the electric field by the magnetic field, all the electric field E_y on the right fine grid of Fig. 3b can be calculated by the difference between H_x and H_z. However, when calculating the electric field E_y at the junction of the coarse and fine grids, there are two magnetic fields H_z on its right side and only one magnetic field on the other side, which does not satisfy the difference scheme. To satisfy the difference condition of equation (10), the magnetic field H_{z1} of the adjacent fine grids (dotted line) can be obtained by interpolation. Then, we can obtain the difference equation of E_y at the boundary of the coarse grids and fine grids.

The grids needed for the binary paraboloid interpolation method are shown in Fig. 4. The coarse grid adjacent to the fine grid is named the central grid, whose magnetic field is H_3. The magnetic fields of other grids, such as the upper grid, lower grid, left grid and right grid, are H_1, H_5, H_2 and H_4, respectively. To calculate the electric field components

$$-[i\omega\mu_0\sigma + \mathbf{C_{HzDy}C_{ExDy}} + \mathbf{C_{HyDz}C_{ExDz}}]\mathbf{E_x} + \mathbf{C_{HzDy}C_{EyDx}E_y} + \mathbf{C_{HyDz}C_{EzDx}E_z} = i\omega\mu_0\mathbf{J_x}, \tag{12}$$

$$\mathbf{C_{HzDx}C_{ExDy}E_x} - [i\omega\mu_0\sigma + \mathbf{C_{HxDz}C_{EyDz}} + \mathbf{C_{HzDx}C_{EyDx}}]\mathbf{E_y} + \mathbf{C_{HxDz}C_{EzDy}E_z} = i\omega\mu_0\mathbf{J_y}, \tag{13}$$

$$\mathbf{C_{HyDx}C_{ExDz}E_x} + \mathbf{C_{HxDy}C_{EyDz}E_y} - [i\omega\mu_0\sigma + \mathbf{C_{HyDx}C_{EzDx}} + \mathbf{C_{HxDy}C_{EzDy}}]\mathbf{E_z} = i\omega\mu_0\mathbf{J_z}, \tag{14}$$

$$\mathbf{x} = \begin{bmatrix} \mathbf{E_x} \\ \mathbf{E_y} \\ \mathbf{E_z} \end{bmatrix}, \tag{15}$$

$$\mathbf{b} = \begin{bmatrix} i\omega\mu_0\mathbf{J_x} \\ i\omega\mu_0\mathbf{J_y} \\ i\omega\mu_0\mathbf{J_z} \end{bmatrix}, \tag{16}$$

$$\mathbf{A} = \begin{bmatrix} -[i\omega\mu_0\sigma + \mathbf{C_{HzDy}C_{ExDy}} + \mathbf{C_{HyDz}C_{ExDz}}] & \mathbf{C_{HzDy}C_{EyDx}} & \mathbf{C_{HyDz}C_{EzDx}} \\ \mathbf{C_{HzDx}C_{ExDy}} & -[i\omega\mu_0\sigma + \mathbf{C_{HxDz}C_{EyDz}} + \mathbf{C_{HzDx}C_{EyDx}}] & \mathbf{C_{HxDz}C_{EzDy}} \\ \mathbf{C_{HyDx}C_{ExDz}} & \mathbf{C_{HxDy}C_{EyDz}} & -[i\omega\mu_0\sigma + \mathbf{C_{HyDx}C_{EzDx}} + \mathbf{C_{HxDy}C_{EzDy}}] \end{bmatrix}. \tag{17}$$

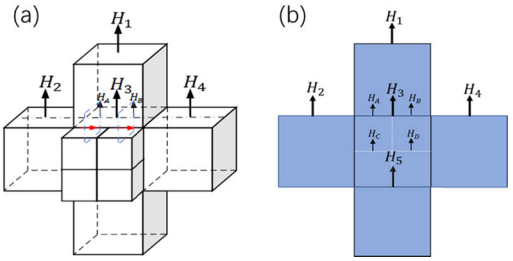

FIGURE 4. The binary paraboloid interpolation method. (a) Stereogram. (b) Profile.

(red arrow) at the boundary of the coarse and fine grids in Fig. 4a, H_A and H_B need to be interpolated. The magnetic fields that need to be interpolated in each grid are shown in Fig. 4b, which are H_A, H_B, H_C and H_D. The interpolation method is shown in equation (22).

$$f(x, y) = ax^2 + by^2 + cx + dy + e. \tag{22}$$

By substituting the magnetic field of the five grids, we can obtain the following equations:

$$\begin{cases} f(0, 0) = e = H_3, \\ f(1, 0) = a + c + e = H_4, \\ f(-1, 0) = a - c + e = H_2, \\ f(0, 1) = b + d + e = H_1, \\ f(0, -1) = b - d + e = H_5. \end{cases} \tag{23}$$

According to equation (23), the parameters, such as a, b, c, d and e, can be obtained as follows:

$$\begin{cases} a = \dfrac{H_4 + H_2 - 2H_3}{2}, \\ b = \dfrac{H_1 + H_5 - 2H_3}{2}, \\ c = \dfrac{H_4 - H_2}{2}, \\ d = \dfrac{H_1 - H_5}{2}, \\ e = H_3. \end{cases} \tag{24}$$

Substituting the parameters obtained in equation (24) into equation (22), we can obtain the required magnetic field equation,

$$f(x, y) = \frac{H_4 + H_2 - 2H_3}{2}x^2 + \frac{H_1 + H_5 - 2H_3}{2}y^2 + \frac{H_4 - H_2}{2}x + \frac{H_1 - H_5}{2}y + H_3. \tag{25}$$

As shown in Fig. 4, we can obtain the interpolation equations of magnetic fields H_A, H_B, H_C and H_D.

$$\begin{cases} H_A = \dfrac{5}{32}H_2 - \dfrac{3}{32}H_4 + \dfrac{15}{16}H_3, \\ H_B = -\dfrac{3}{32}H_2 + \dfrac{5}{32}H_4 + \dfrac{15}{16}H_3, \\ H_c = \dfrac{5}{32}H_2 - \dfrac{3}{32}H_4 - \dfrac{1}{8}H_1 + \dfrac{3}{8}H_5 + \dfrac{11}{16}H_3, \\ H_D = -\dfrac{3}{32}H_2 + \dfrac{5}{32}H_4 - \dfrac{1}{8}H_1 + \dfrac{3}{8}H_5 + \dfrac{11}{16}H_3. \end{cases} \tag{26}$$

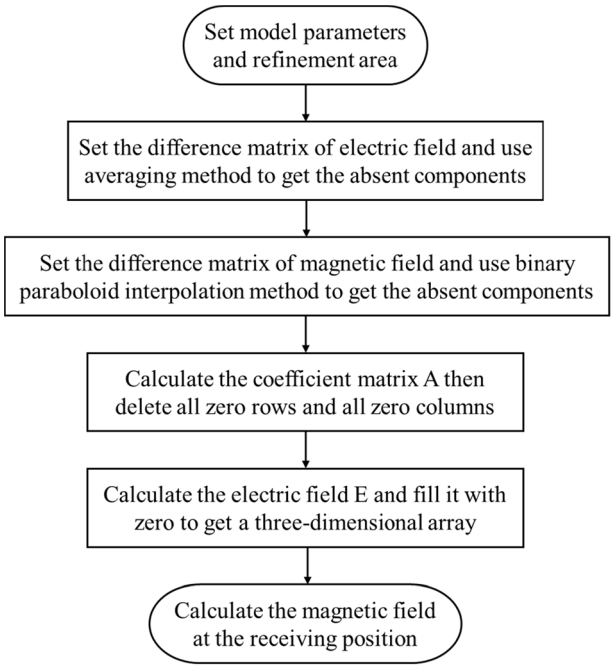

FIGURE 5. Flowchart of the calculation.

Finally, the calculation procedure of response at each frequency point can be summarized as follows, and Fig. 5 shows the flowchart:

III. ACCURACY VERITIFICATION

To verify the correctness of the FDFD method based on octree grids, we adopt a transmitting loop source and a receiver in the center of the loop to calculate the responses of a homogeneous earth model, four classical layered earth models and an earth model with a low-resistivity anomaly. For the boundary, we use the Dirichlet conditions. The computational region consists of grids of different sizes. Variable step-size grids are used in the outer layer, and uniform grids are used in the central region.

A. COMPARISON OF THE SOLUTIONS OF THE HOMOGENEOUS EARTH MODEL

The analytical solution [31] of the vertical magnetic field of a homogeneous half-space model in the frequency domain can be expressed as follows:

$$H_z = -\frac{I}{k^2a^3}[3 - (3 + 3ika - k^2a^2)e^{-ika}]. \tag{27}$$

where $k = \sqrt{-i\omega\mu\sigma}$, the earth conductivity is $\sigma = 0.01$ S/m, the transmitting current is $I = 1$A, and the permeability is $\mu = 4\pi * 10^{-7}$H/m. The transmitting coil is a square loop with a side length of 100 m; then, we can obtain $a = \sqrt{100^2/\pi}$ by the equivalence principle. The computational region consists of $30 \times 30 \times 30$ grids. The model parameters and grid sectional view are shown in Fig. 6. In the center region, we use uniform grids with a size of 10 m. Octree grids are positioned 30 m below the coil, whose minimum grid size is 5 m, and the length, width and height of the refined regions are 40 m, 20 m

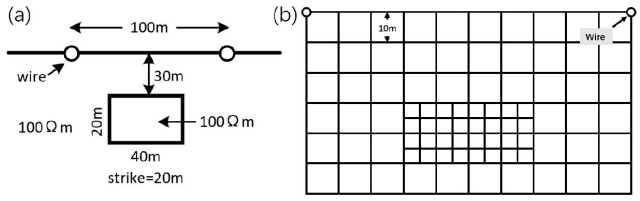

FIGURE 6. (a) Homogeneous earth model. (b) Octree grid sectional view.

and 20 m, respectively. Considering that the earth model is homogeneous, we set the conductivity of the octree region to be the same as that of the other regions. A comparison between the FDFD numerical solution and the analytical solution in the frequency domain is shown in Fig. 7a, and the relative error curve is shown in Fig. 7b. Within 10^4 Hz, the relative error of the imaginary part is less than 1%. As the frequency increases, the skin depth becomes shallow, which leads to an increase in the relative error.

We use digital filtering techniques to obtain the solution in the time domain. Then, we compare the response with the half-space analytical solution [31]. The equation of the analytical solution in the time domain is shown as follows:

$$H_z = \frac{I}{2a}\left[\frac{3}{\sqrt{\pi}\theta a}e^{-\theta^2 a^2} + \left(1 - \frac{3}{2\theta^2 a^2}\right)\mathrm{erf}(\theta a)\right]. \quad (28)$$

where erf is the error function and $\theta = \sqrt{\mu\sigma/(4\mathrm{t})}$. Other parameters, such as a, I and σ, are the same as those in equation (27). A comparison of the numerical solution based on octree grids and the analytical solution in the time domain is shown in Fig. 8a. The relative error is shown in Fig. 8b and the maximum error is less than 4%.

B. COMPARISON OF THE FDFD SOLUTIONS WITH DIGITAL FILTER SOLUTIONS FOR THE LAYERED EARTH MODELS

To verify the correctness of the algorithm, we calculate the electromagnetic responses of four typical three-layer models, A, H, K and Q. Then, we compare the responses with the digital filter solutions. In addition to the conductivity parameters, the other parameters of the layered earth model are the same as those of the previous homogeneous half-space model. The uniform grids with a size of 25 m are used in the central region. The refined area based on octree grids is located at the center of the second layer of the earth, whose minimum grids are 12.5 m, and the conductivity is the same as that of the other region. This refined area is located 125 m below the coil, and the length, width and height of the refined regions are 100 m, 50 m and 50 m. The specific parameters for each layer are shown in Fig. 9, and the two curves in each picture basically coincide. The average relative errors of the A, H, K and Q models are 2.99%, 3.58%, 3.39% and 2.26%, respectively. The maximum relative errors of the A, H, K and Q models are 10.01%, 6.99%, 6.48% and 6.63%, respectively.

C. COMPARISON OF THE SOLUTIONS OF THE EARTH MODEL WITH A LOW-RESISTANCE ANOMALOUS BODY

To verify the correctness of the algorithm, we calculate the solutions based on octree grids and Yee grids. Then we compare our solutions with the solutions calculated by the FDTD method [2] and the integral equation method [6]. The comparison and the model parameters are shown in Fig. 10a. In the papers on the FDTD method and integral equation method, only 0.1 ms-10 ms solutions are given; we present the solutions between 0.01 ms-10 ms. The side length of the square transmitting loop is 100 m. The earth background resistivity is 10 Ω . m. The length, width and height of the anomalous body are 100 m, 40 m and 30 m, respectively, and the resistivity is 0.5 Ω . m. The position of the anomalous body is 30 m below the right side of the loop source. The FDFD response curve (green line) is calculated by the FDFD method based on uniform grids. The octree FDFD response curve (black line) is calculated by the FDFD method based on octree grids. As shown in Fig. 10b, uniform grids are used in the central computing area, and octree grids are used in the area where the anomalous body is located to further refine the grid. Comparing the response curves of the four different algorithms in Fig. 10a, we can see that the results of the four algorithms are basically the same. The three curves calculated by the FDFD method based on octree grids, the FDFD method based on uniform grids and the FDTD method basically coincide. Slight upward warping of the curve can be observed between 0.1 ms and 1 ms, which shows that the anomalous body slows down the diffusion of the electromagnetic field. The accuracy of the results of the FDFD method based on octree grids is verified by comparison.

IV. COMPUTATION EFFICIENCY COMPARISION

The FDFD method needs to solve large linear equations in the calculation process. The number of grids has a considerable influence on the time required for the calculation. To compare the computational efficiencies of the FDFD method based on octree grids and those based on Yee grids, we use the earth models of the L-shaped and trapezoidal low-resistivity anomalous bodies with different grids, and then compare the computing times.

First, we use the FDFD method based on the Yee grids to calculate the response of the earth model with the same frequency and the similar number of grids, and then compare the computational time with that of the other two scholars. (1) Newman [16] used a horizontal magnetic dipole source to calculate a uniform earth model, whose resistivity is 100 Ω.m, with 114264 grids at 30 kHz. The computational time is 2469 s. For comparison, we used a loop source to calculate a similar earth model with 110592 ($48 \times 48 \times 48$) grids at the same frequency. The computational time is 817 s. (2) Han [32] used a long wire source to calculate a seabed layered model with 46656 ($32 \times 27 \times 54$) grids at 1 Hz. The depth of the first two layers of the model are 1000 m and 100 m, and the resistivity of each layer is 1 Ω . m, 100 Ω . m and 1 Ω . m. The computational time with a single thread is approximately 6.8 minutes. Considering the parameter difference between the seabed model and the earth model studied, the resistivity of the earth model we calculated is changed to 100 Ω . m,

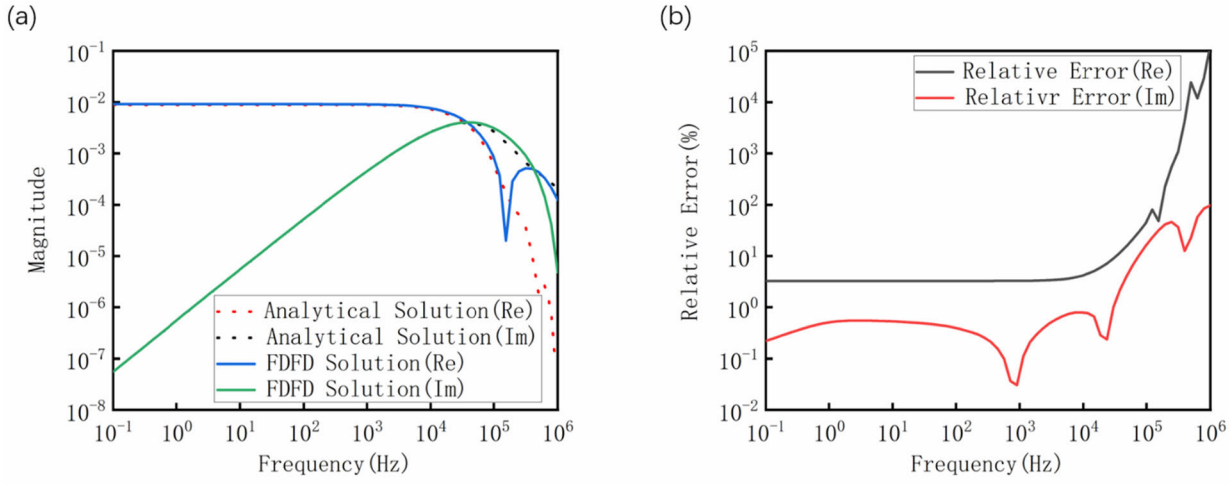

FIGURE 7. Comparison of the solutions of the uniform earth model in the frequency domain. (a) Comparison of numerical and analytical solutions in the frequency domain. (b) Relative error.

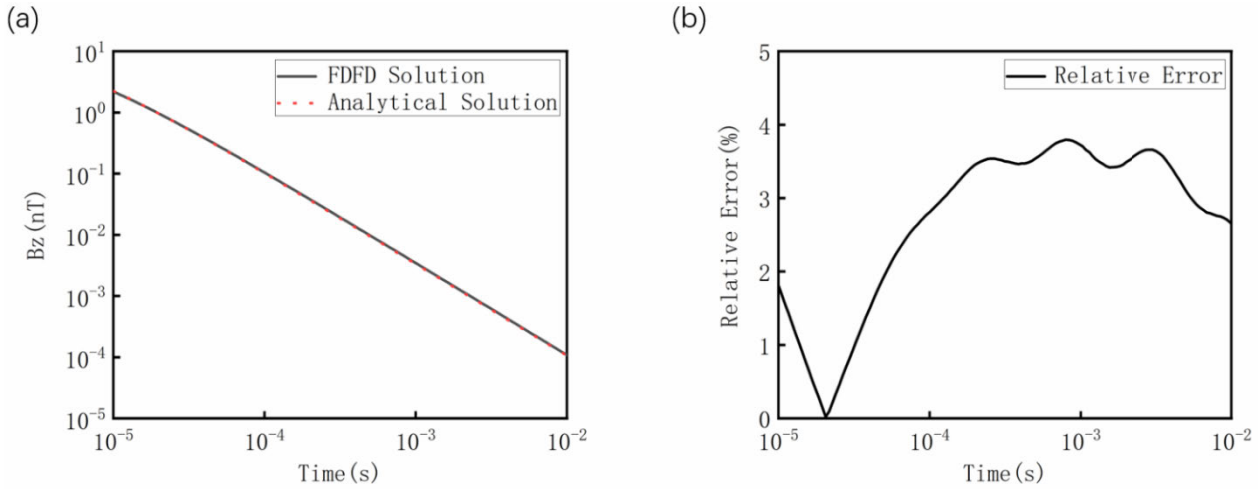

FIGURE 8. Comparison of the solutions of the uniform earth model in the time domain. (a) Comparison of the numerical and analytical solutions in the time domain. (b) Relative error.

1 $\Omega \cdot m$ and 100$\Omega \cdot m$, while the depth of each layer of the earth model is the same as that of the seabed model. We used a loop source to calculate the earth model with 48384 ($32 \times 28 \times 54$) grids at the same frequency, and the calculation time is approximately 3.3 minutes.

The result is shown in Fig. 11a is the L-shaped earth model. The computational time at each frequency point is shown in Fig. 11b. The model subsection profiles by the uniform grids and octree grids are shown in Fig. 11c and Fig. 11d, respectively. The transmitting coil is a square loop with a side length of 80 m and the transmitting current of $I = 1$A. The receiver is in the center of the loop. An L-shaped low-resistivity anomalous body, whose resistivity is 2 $\Omega \cdot$ m, is positioned 30 m below the coil. The resistivity of the earth background is 100 $\Omega \cdot m$. The response curve shows that the prominence is obvious at 0.1 ms, which clearly shows the existence of an anomalous body and the reduction in the attenuation rate of the response curve. The two curves basically coincide, while the average relative error is 4.54%, and the maximum relative error is 6.45%. By comparing the two curves, it is shown that the octree grids have the same effect as that of the Yee grids. The electromagnetic response profile in Fig. 12 clearly reflects the characteristics of electromagnetic field diffusion. Slices are made at Y = 2550 m, 2600 m and 2650 m. We can see that the low-resistance anomalous body slows down the diffusion of the electromagnetic field, and the outline of the anomalous body can be clearly seen at the position of approximately Z = −30 m. A comparison of the average computational times for the two kinds of grids, which is obtained by averaging the computational time of 70 frequency points, is shown in Table 1. As the calculation results are basically consistent, we can see that using octree grids to partition anomalous bodies can significantly reduce the computational time.

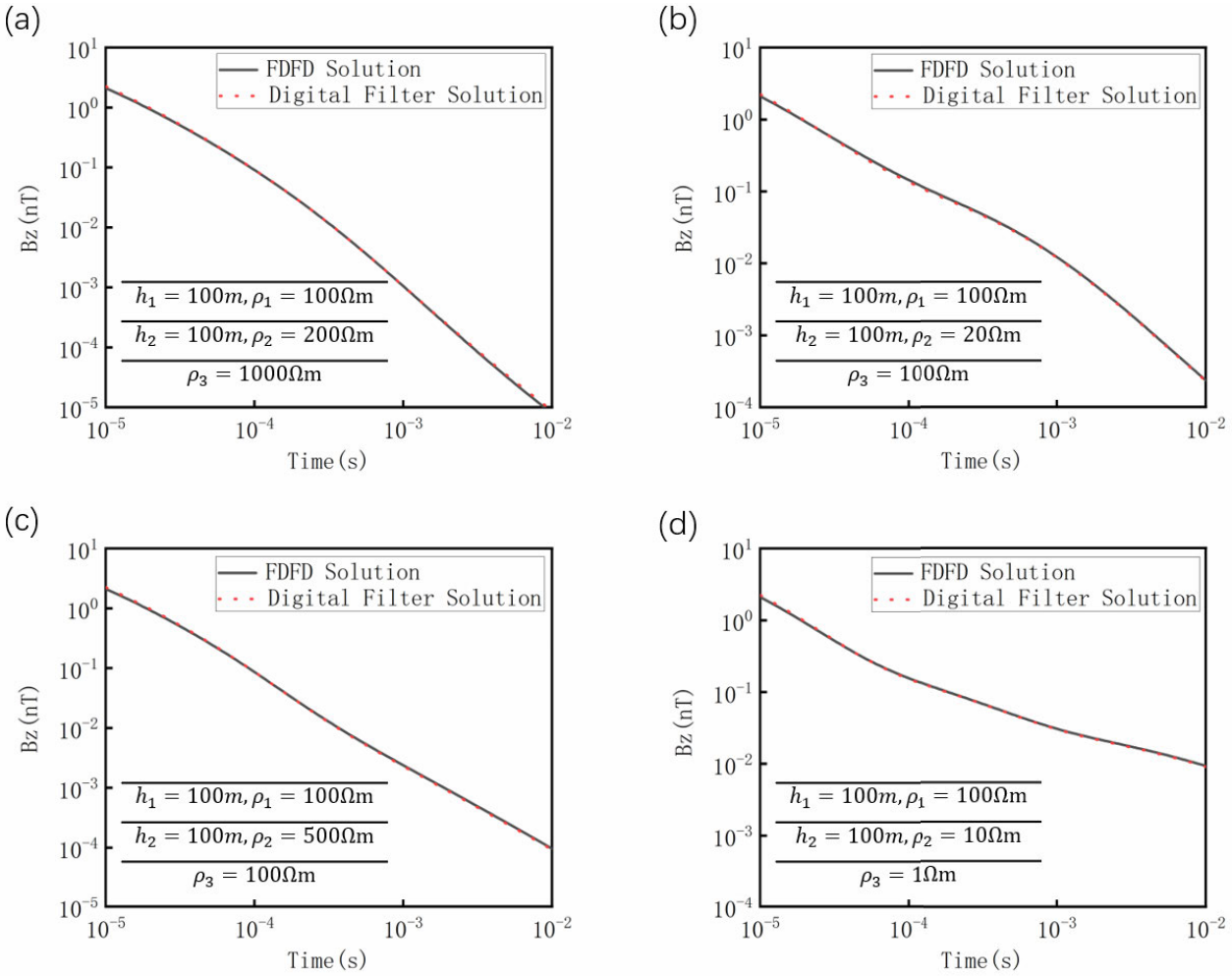

FIGURE 9. Comparisons of the numerical solutions and digital filter solutions of the four-layered earth models. (a) A-type layered earth model. (b) H-type layered earth model. (c) K-type layered earth model. (d) Q-type layered earth model.

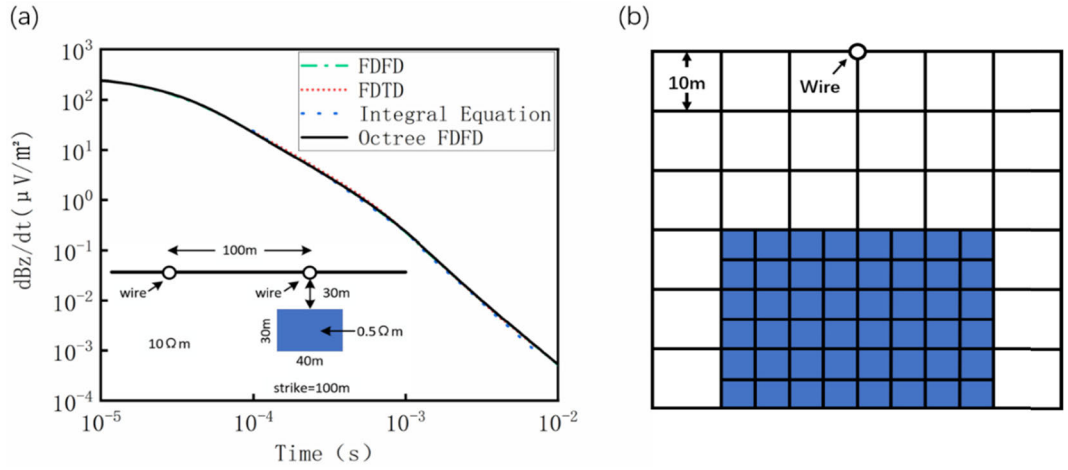

FIGURE 10. Comparison of the solutions of the earth model with a three-dimensional anomalous body. (a) Comparison of the response curves. (b) Octree grids sectional view.

For irregular edge-shaped anomalous bodies, we can perform a local refinement for the irregular parts. Fig. 13a shows an earth model with a trapezoidal anomalous body. We use an 80 m × 80 m transmitting loop source whose current is 1 A

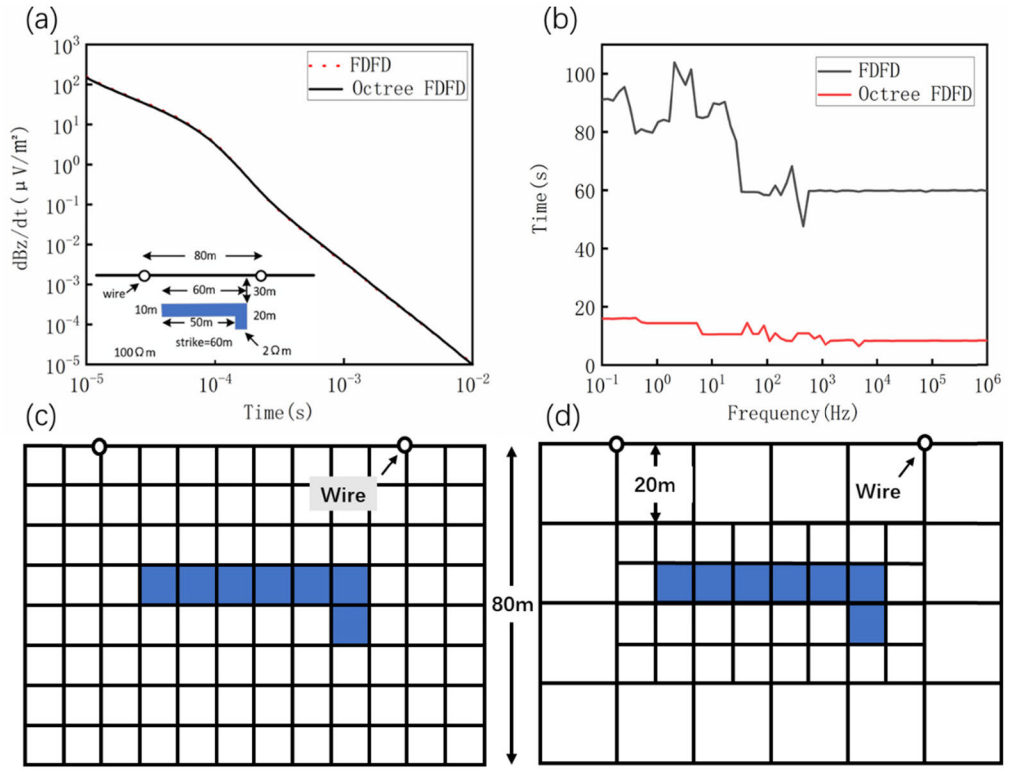

FIGURE 11. Comparison of the L-shaped anomalous bodies. (a) Comparison of the response curves. (b) Comparison of the computational time. (c) Uniform grid sectional view. (d) Octree grid sectional view.

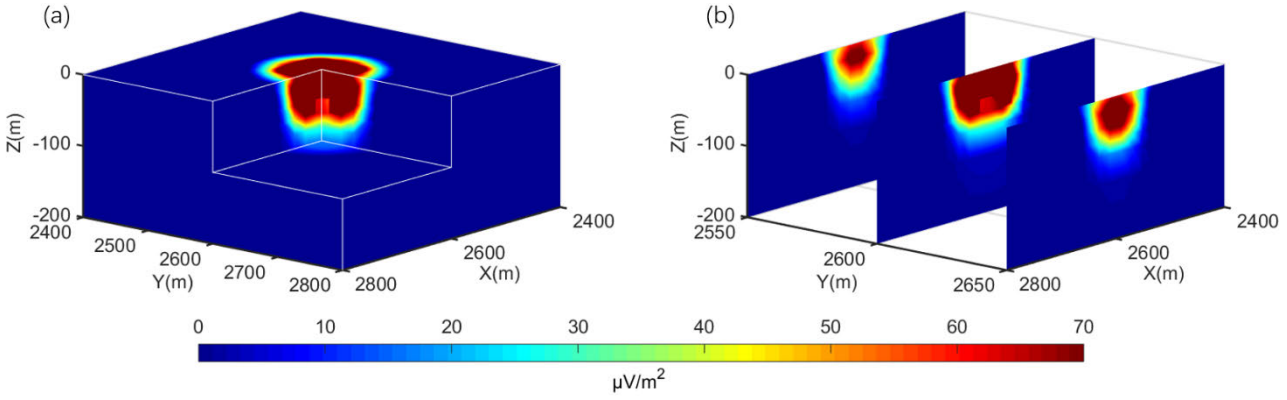

FIGURE 12. Sectional view and slice diagrams of the L-shaped anomalous body (a) Sectional view of the electromagnetic response of the L-shaped anomalous body at t=0.01ms (b) Slice diagrams of Y = 2550 m, 2600 m and 2650 m at t = 0.01 ms.

TABLE 1. Comparisons of the grids.

Grids	Number	Size	Average Time
FDFD	30×30×30	10 m	69.8 s
Octree FDFD	20×20×20	20 m	10.7 s

and a receiver in the center of the loop. There is a trapezoidal low-resistivity anomalous body 20 m below the coil, whose resistivity is 10 $\Omega \cdot m$. The earth background resistivity is 100 $\Omega \cdot m$. The computational time at each frequency point is shown in Fig. 13b.The response curves calculated for the Yee grids and octree grids are shown in Fig. 13c and Fig. 13d, respectively. Then, we compare their computational times.

From the calculation results in Fig. 13a, the decreasing rate of the curve slows down in the period of 0.01 ms-0.1 ms, which accurately reflects the existence of a low-resistance anomalous body. As the two curves basically coincide, the average relative error and the maximum relative error are 2.69% and 6.96%, respectively, which satisfy the accu-

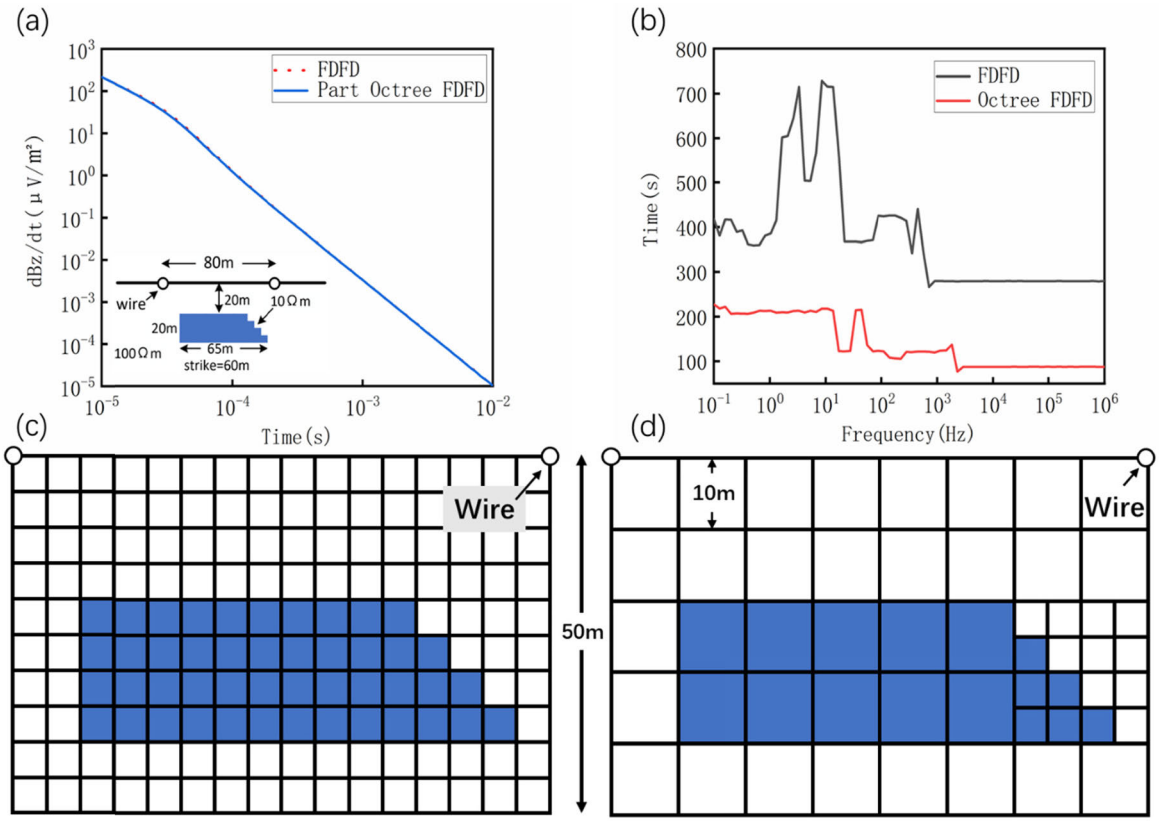

FIGURE 13. Comparison of the trapezoidal anomalous bodies. (a) Comparison of the response curves. (b) Comparison of the computational time. (c) Uniform grid sectional view. (d) Octree grid sectional view.

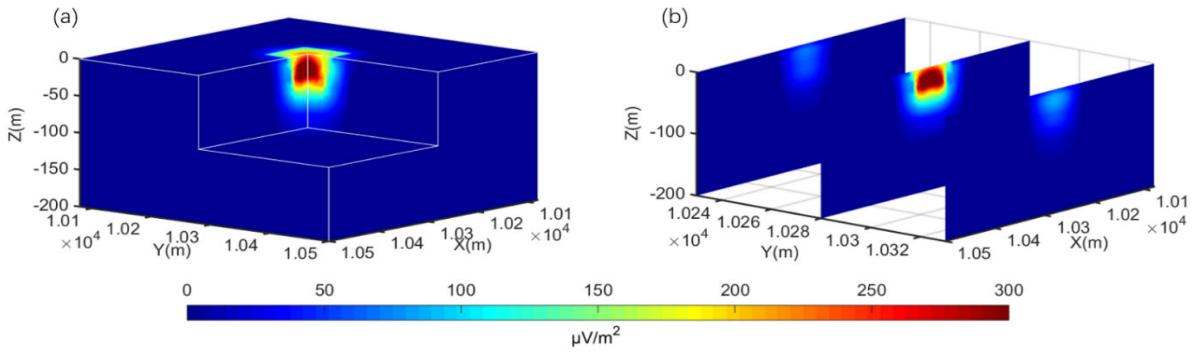

FIGURE 14. Sectional view and slice diagrams of the trapezoidal anomalous body. (a) Sectional view of the electromagnetic response of the trapezoidal model at t=0.01 ms. (b) Slice diagrams of Y=10230 m, 10280 m and 10330 m at t=0.01 ms.

racy requirements. From the electromagnetic response sectional view of Fig. 14, the electromagnetic field is obviously slowed down when it diffuses to approximately $Z = -20$ m. Then, we calculate slice diagrams along the Y direction at $Y = 10230$ m, 10280 m and 10330 m. The electromagnetic field diffuses quickly on both sides and slowly in the middle, and the existence of an anomalous body is recognized. A comparison of the average computational times for the two kinds of grids is shown in Table 2. The octree grids are used to refine the irregular part of the complex anomalous body, which can effectively reduce the computational time compared to that of the Yee grids. When the computational region is the same, the FDFD method based on octree grids

TABLE 2. Comparisons of the grids.

Grids	Number	Size	Average Time
FDFD	40×40×40	5 m	376 s
Part Octree FDFD	30×30×30	10 m	139 s

takes only 37% of the time of the Yee grids. Above all, the octree grid can effectively reduce the computational time and improve the computational efficiency while ensuring the accuracy of the calculation.

V. CONCLUSION AND DISCUSSION

The number of grids in the FDFD method is the key factor in the computational time. More grids are needed to calculate the electromagnetic response of a complex anomalous body, and the computational time is longer. To solve this problem, the FDFD method is combined with octree grids to reduce the number of grids required. Specifically, based on the premise of a sufficiently large computational area, the size of the coarse grid is unchanged, and the minimum grid size is reduced by half. The octree grid used in the FDFD method effectively reduces the number of grids needed for the simulation and improves the computational efficiency. The main conclusions of this paper are as follows:

(1) In the numerical simulation, the data storage problem of the octree grid in the FDFD method is solved. Based on fine grids, the element vacancies of the coarse grid are set to 0, and the grid size, electric field components and magnetic field components are arranged in an orderly manner.

(2) The problem of electromagnetic field component transfer at the boundary of the coarse grid and fine grid is solved. More specifically, the electric field components of the coarse grid are obtained by an average method, and the magnetic field components are obtained by the binary paraboloid interpolation method.

(3) The FDFD method based on octree grids is used to calculate the electromagnetic response of a uniform earth model, four typical layered models and a three-dimensional low-resistivity anomalous body model, which verifies the correctness of the algorithm.

(4) The electromagnetic responses of L-shaped and trapezoidal anomalous bodies are calculated by using the FDFD method based on octree grids and Yee grids. According to the comparison of the results, we find that the octree grid can effectively reduce the computing time and improve the computational efficiency while ensuring computational accuracy.

The FDFD method takes much time in solving large linear equations, and the solving process of each frequency point is independent. Therefore, the next step is to adopt parallel algorithms based on MPI (message passing interface) to further improve computational efficiency.

REFERENCES

[1] C. Yu, X. Liu, and E. Li, "Mapping the mined-out area saturated by water with transient electromagnetic method," in *Proc. ICEEP*, vol. 170, 2018, pp. 1625–1629.

[2] T. Wang and G. W. Hohmann, "A finite-difference, time-domain solution for three-dimensional electromagnetic modeling," *Geophysics*, vol. 58, no. 6, pp. 797–809, 1993.

[3] F. Assous, P. Degond, E. Heintze, P. A. Raviart, and J. Segre, "On a finite-element method for solving the three-dimensional Maxwell equations," *J. Comput. Phys.*, vol. 109, pp. 222–237, Dec. 1993.

[4] S. Yang, Y. Yu, Z. Chen, and S. Ponomarenko, "A time-domain collocation meshless method with local radial basis functions for electromagnetic transient analysis," *IEEE Trans. Antennas Propag.*, vol. 62, no. 10, pp. 5334–5338, Oct. 2014.

[5] X. Lu, C. G. Farquharson, J.-M. Miehé, and G. Harrison, "3D finite-volume time-domain electromagnetic modeling of the close lake graphitic faults using unstructured grids," in *Proc. 88th Annu. Meeting SEG Int. Expo.*, 2018, pp. 1908–1912.

[6] G. A. Newman, G. W. Hohmann, and W. L. Anderson, "Transient electromagnetic response of a three-dimensional body in a layered earth," *Geophysics*, vol. 51, no. 8, pp. 1608–1627, 1986.

[7] K. S. Kunz and R. J. Luebbers, *The Finite Difference Time Domain Method for Electromagnetics*. Boca Raton, FL, USA: CRC Press, 1993.

[8] R.-U. Börner, "Numerical modelling in geo-electromagnetics: Advances and challenges," *Surv. Geophys.*, vol. 31, no. 2, pp. 225–245, 2010.

[9] W. Sha, Z. Huang, M. Chen, and X. Wu, "Survey on symplectic finite-difference time-domain schemes for Maxwell's equations," *IEEE Trans. Antennas Propag.*, vol. 56, no. 2, pp. 493–500, Feb. 2008.

[10] V. Singh, "A finite difference frequency domain based full vectorial transverse modesolver for anisotropic waveguides with arbitrary permittivity and permeability tensors," *ACES J.*, vol. 33, no. 7, pp. 806–809, 2018.

[11] T.-M. Huang, T. Li, W.-D. Li, J.-W. Lin, W.-W. Lin, and H. Tian, "Solving three dimensional Maxwell eigenvalue problem with fourteen Bravais lattices," 2018, *arXiv:1806.10782*. [Online]. Available: https://arxiv.org/abs/1806.10782

[12] T. Szarvas and Z. Kis, "Numerical simulation of nonlinear second harmonic wave generation by the finite difference frequency domain method," *J. Opt. Soc. Amer. B, Opt. Phys.*, vol. 35, no. 4, pp. 731–740, 2018.

[13] C. de Groot-Hedlin, "Finite-difference modeling of magnetotelluric fields: Error estimates for uniform and nonuniform grids," *Geophysics*, vol. 71, no. 3, pp. G97–G106, 2006.

[14] D. Yoon, M. S. Zhdanov, J. Mattsson, H. Cai, and A. Gribenko, "A hybrid finite-difference and integral-equation method for modeling and inversion of marine controlled-source electromagnetic data," *Geophysics*, vol. 81, no. 5, pp. E323–E336, 2016.

[15] G. Li, Y. Li, and B. Han, "Accurate interpolation at receiver positions: A novel method for frequency-domain marine CSEM finite-difference modelling," *Pure Appl. Geophys.*, vol. 174, no. 5, pp. 2143–2160, 2017.

[16] G. A. Newman and D. L. Alumbaugh, "Frequency-domain modelling of airborne electromagnetic responses using staggered finite differences," *Geophys. Prospecting*, vol. 43, pp. 1021–1042, Nov. 1995.

[17] K. Yee, "Numerical solution of initial boundary value problems involving Maxwell's equations in isotropic media," *IEEE Trans. Antennas Propag.*, vol. AP-14, no. 3, pp. 302–307, May 1966.

[18] J. Xu and G. Xie, "A novel hybrid method of spatially filtered FDTD and subgridding technique," *IEEE Access*, vol. 7, pp. 85622–85626, 2019.

[19] Z. Ye, C. Liao, X. Xiong, and M. Zhang, "A novel FDTD subgridding method with improved separated temporal and spatial subgridding interfaces," *IEEE Antennas Wireless Propag. Lett.*, vol. 16, pp. 1011–1015, 2017.

[20] A. Valente, F. Loureiro, L. Di Bartolo, and W. J. Mansur, "Computer simulation of hyperthermia with nanoparticles using an OcTree finite volume technique," *Int. Commun. Heat Mass Transf.*, vol. 91, pp. 248–255, Feb. 2018.

[21] H. Abe, "Blocked adaptive Cartesian grid FD-TD method for electromagnetic field with complex geometries," in *Proc. Int. Conf. Modeling Simulation Technol.*, 2011, pp. 155–161.

[22] S. Popinet, "Gerris: A tree-based adaptive solver for the incompressible Euler equations in complex geometries," *J. Comput. Phys.*, vol. 190, pp. 572–600, Sep. 2003.

[23] E. Haber and S. Heldmann, "An octree multigrid method for quasi-static Maxwell's equations with highly discontinuous coefficients," *J. Comput. Phys.*, vol. 223, no. 2, pp. 783–796, 2007.

[24] L. Horesh and E. Haber, "A second order discretization of Maxwell's equations in the quasi-static regime on octree grids," *SIAM J. Sci. Comput.*, vol. 33, no. 5, pp. 2805–2822, 2011.

[25] A. Valente, L. Di Bartolo, and W. J. Mansur, "3D seismic modeling using staggered-grid OcTree mesh," in *Proc. SEG New Orleans Annu. Meeting*, 2015, pp. 3754–3758.

[26] M. Theillard, C. H. Rycroft, and F. Gibou, "A multigrid method on non-graded adaptive octree and quadtree Cartesian grids," *J. Sci. Comput.*, vol. 55, no. 1, pp. 1–15, 2013.

[27] C. Min, F. Gibou, and H. D. Ceniceros, "A supra-convergent finite difference scheme for the variable coefficient Poisson equation on non-graded grids," *J. Comput. Phys.*, vol. 218, pp. 123–140, Oct. 2006.
[28] Y. Yin, "Research on the microstructure simulation of the alloy solidification based on phase field method by the octree mesh technology," Ph.D. dissertation, Huazhong Univ. Sci. Technol., Wuhan, China, Jun. 2013.
[29] A. Raeli, M. Bergmann, and A. Iollo, "A finite-difference method for the variable coefficient Poisson equation on hierarchical Cartesian meshes," *J. Comput. Phys.*, vol. 355, pp. 59–77, Feb. 2018.
[30] A. Y. Chernyshenko, M. A. Olshanskii, and Y. V. Vassilevski, "A hybrid finite volume—Finite element method for bulk–surface coupled problems," *J. Comput. Phys.*, vol. 352, pp. 516–533, Jan. 2018.
[31] M. N. Nabighian, *Electromagnetic Methods in Applied Geophysics: Theory*, vol. 1. Tulsa, OK, USA: Society of Exploration Geophysicists, 1992, pp. 208–209.
[32] B. Han, X. Y. Hu, Y. F. Huang, R. H. Peng, J. Li, and J. C. Cai, "3-D frequency-domain CSEM modeling using a parallel direct solver," *Chin. J. Geophys.*, vol. 58, no. 8, pp. 2812–2826, 2015.

HUI LUAN was born in Baishan, Jilin, China, in 1979. She received the B.S. degree in computer science and technology from Harbin Engineering University, China, in 2001, and the Ph.D. degree in microwave remote sensing from the Chinese Academy of Science, China, in 2007. Her work focuses on electromagnetic numerical simulation.

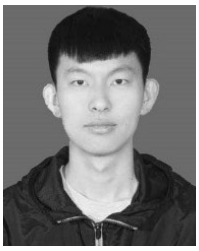

YINAN GENG was born in Hebei, China, in 1993. He received the B.S. degree from the School of Electrical Engineering and Automation, Jilin University, China, in 2016, where he is currently pursuing the M.S. degree. His research interest includes frequency-domain numerical simulation.

YIBING YU received the bachelor's degree in electrical engineering from the College of Instrumentation and Electrical Engineering, Jilin University, China, in 2017. He is currently pursuing the Ph.D. degree in electrical theory and new technology. His research interest includes numerical simulation.

SHANSHAN GUAN received the Ph.D. degree in measuring and testing technology and instrument from Jilin University, Changchun, China, in 2012. In 2019, she was a Visiting Scholar with the Southern University of Science and Technology, China. Since 2012, she has been with the College of Instrumentation and Electrical Engineering, Jilin University, where she is currently an Associate Professor. Her research interests include the development of transient electromagnetic instruments and data forward, and inverse algorithms.